



AIAA CP 2001-0993

**Transient Rotor Inflow Using a
Time-Accurate Free-Vortex Wake Model**

Mahendra J. Bhagwat

J. Gordon Leishman

Department of Aerospace Engineering,

Glenn L. Martin Institute of Technology,

University of Maryland, College Park, Maryland 20742

**39th AIAA Aerospace Sciences
Meeting & Exhibit**

8–11 January 2001 / Reno, NV

Transient Rotor Inflow Using a Time-Accurate Free-Vortex Wake Model

Mahendra J. Bhagwat*

J. Gordon Leishman†

Department of Aerospace Engineering,
Glenn L. Martin Institute of Technology,
University of Maryland, College Park, Maryland 20742

A time-marching free-vortex wake analysis was developed for application to the prediction of the aerodynamics of a helicopter rotor under transient or maneuvering flight conditions. The stability, accuracy and convergence of the time-marching algorithms was rigorously examined. A linearized analysis was used to determine the basic stability characteristics of the algorithms. A new time-marching algorithm is proposed to ensure numerical stability and convergence of the wake solution. The second-order accuracy and grid independent nature of the wake geometry solution is demonstrated. This algorithm is applied to the problem of transient rotor response resulting from time-varying changes in the rotor collective pitch inputs. Good agreement is shown between the predictions and experimental measurements.

Nomenclature

c	blade chord, m
$C_{l\alpha}$	lift curve slope, rad^{-1}
dL	elemental blade lift, N
e	flapping hinge offset, m
h	time marching step, $= \Delta t$, s
I_β	blade flapping moment of inertia, kg m^2
m_a	apparent mass term in dynamic inflow, kg
M_β	blade flapping moment, N m
N_b	number of blades
\vec{r}	position vector of vortex collocation point, m
R	rotor radius, m
t	time, s
\vec{V}	velocity vector, ms^{-1}
v_i	rotor induced velocity, ms^{-1}
V_∞	freestream velocity, ms^{-1}
$\Delta\psi$	azimuthal discretization, rad
$\Delta\zeta$	vortex age discretization, rad
β	blade flap angle, rad
β_p	precone angle, rad
Γ	vortex strength (circulation), m^2s^{-1}
λ_i	inflow ratio, $= v_i/\Omega R$
μ	advance ratio, $= V_\infty/\Omega R$
ν_β	non-dimensional blade flapping frequency
θ	rotor collective pitch, rad
ρ	fluid (air) density, kg m^{-3}
σ	eigenvalue of time-integration method, s^{-1}
τ	time-constant for inflow build-up, s^{-1}
Ω	rotor rotational speed, rad s^{-1}
ψ	azimuth angle, rad
ψ_b	blade azimuthal location, rad
ζ	vortex age, rad

Introduction

Over the past three decades, free-vortex methods have emerged as robust and versatile tools for modeling the complicated vortical wake structure trailed from a helicopter rotor. The advantage of free-vortex methods is that they solve for the force-free positions of the discrete vortex elements in the wake, thereby enabling more accurate predictions of the non-uniform induced velocity field, both at the rotor disk and elsewhere in the flow such as near the airframe. Therefore, their use usually leads to better predictions of rotor loads, rotor performance, rotor vibration levels, airframe loads and also the acoustics of the aircraft. Free-vortex wake methods are now relatively mature, and have been successfully applied in several types of rotor aeromechanical analyses under steady flight conditions. However, for reasons related to their formulation and/or numerical behavior, they are usually inadequate for use under transient flight conditions such as tight-turns, pitch-ups and other important maneuvers. Because the maneuvering flight capability limits the performance of the modern helicopter, better time-accurate vortex methods must be developed to predict the rotor airloads under these conditions.

The dynamic response of the wake and the induced velocity field surrounding a helicopter rotor during transient or maneuvering flight is yet to be fully understood. The highly vortical nature of the rotor wake¹ leads to a complicated, three-dimensional, induced velocity field, even under steady flight conditions. It is, therefore, to be expected that the dynamics of the rotor wake plays a significant role in determining the transient aerodynamic response of the rotor to time-varying motion, such as for pitch or roll rates or other types of transient inputs to the rotor. Recent literature (e.g., Refs. 2–4) stresses the increasing need for improved time-accurate rotor wake models for airloads and other aeromechanical applications. It has been observed that significant differences between flight mechanics simula-

*Graduate Research Assistant. <mrb@eng.umd.edu>

†Professor. <leishman@eng.umd.edu>

Copyright © 2001 by the American Institute of Aeronautics and Astronautics, Inc. All rights reserved.

tions and in-flight experiments, especially for the so-called “off-axis” blade flapping response found during maneuvering flight, can be related to inaccurate, or incomplete, modeling of the transient aerodynamics of the rotor wake, e.g. Ref. 2.

The development of time-accurate free-vortex wake models suitable for application to maneuvering flight conditions has historically been a challenging task for the rotor analyst. One reason is that time-accurate rotor wake calculations have been found to be susceptible to different types of numerical instabilities, especially in hovering flight, where the wake geometry does not easily converge to an equilibrium wake geometry solution.⁵⁻⁷ It is sometimes argued that this behavior reflects the inherent physical nature of helicopter rotor wakes, where experimental observations, e.g. Refs. 8, 9 & 10, have shown that the intertwining tip vortex filaments can exhibit several long and/or short wave types of instabilities. Yet, experience has shown that the magnitude of these physical disturbances are generally much smaller than those that have been predicted using time-accurate free-vortex wake calculations (e.g., see Ref. 11). This observation reflects an intrinsic difficulty with these types of solution methodologies, and one that has not yet been completely resolved.

One approach that has been successful in controlling the various non-physical wake instabilities that are known artifacts of the solution process, is to explicitly enforce wake periodicity, e.g., by using influence coefficient based methods,^{6,7} and semi-implicit¹² or pseudo-implicit methods.¹³⁻¹⁶ Further significant improvements in the stability of the schemes are obtained using steady-state solution methods that employ velocity field averaging.¹³⁻¹⁶ However, the explicit enforcement of periodicity limits the rotor wake analysis mainly steady-state or low-rate (non-transient) maneuvering flight conditions. Furthermore, the enforcement of periodicity may artificially suppress any physical transient behavior of the rotor wake, potentially leading to misleading predictions of rotor airloads and performance. Therefore, it is imperative to develop a robust time-accurate wake methodology that is both accurate *and* stable, i.e., it is not susceptible to any types of numerical instabilities.

The principal objective of the present article is to describe and validate the behavior of a stable, convergent, time-accurate free-vortex wake methodology. Time-integration algorithms for solving the time-dependent wake structures were examined using rigorous stability and convergence criteria. In the past, the choice of time-accurate free wake algorithms was based on accuracy considerations. However, unless the algorithm is known to be stable, the numerical solution will not exhibit the expected order of accuracy. Therefore, the present algorithm was examined using both a linear stability criterion and also modified equations to ensure stability. Solution convergence with increasing grid refinement is also demonstrated for both hovering and forward flight. The methodology is then validated against experimental measurements documenting the

rotor response under transient flight conditions with time-varying blade pitch inputs.

Methodology

Blade Flapping Equation of Motion

To determine the transient rotor response, i.e., the aerodynamic loads and the rotor orientation in an inertial frame, the inherent coupling between blade flapping and the wake evolution must be considered. The position of the blade(s), which is governed by the dynamics of its flapping motion, forms a boundary condition for the origin of the vortical wake trailed behind each blade. Therefore, for transient or maneuvering conditions it is necessary to integrate the flapping equation of motion for the blade(s) in a manner that is properly coupled to the equations modeling the rotor wake. The equation of motion of a flapping blade is given by the equilibrium of moments about the flapping hinge - see Refs. 17 or 18 for the complete derivation. For a rigid rotor blade the equation of motion is given by

$$\ddot{\beta} + v_{\beta}^2 \dot{\beta} = \frac{M_{\beta}}{I_{\beta} \Omega^2} + \frac{\omega_0^2}{\Omega^2} \beta_p \quad (1)$$

where the (*) denotes a derivative with the blade azimuth, ψ , and v_{β} is the non-dimensional flapping frequency about the hinge, ω_0 is the non-rotating flap frequency, and β_p is the precone angle of the blades. The flapping moment on the RHS of Eq. 1 is the aerodynamic moment about the hinge as given by

$$M_{\beta} = \int_e^R (r - e) dL \quad (2)$$

where dL is the elemental lift on a spanwise blade element. Because the elemental lift depends on the local induced inflow, the blade flapping response is dictated by the induced velocity field produced by the vortical wake solution. Also, through the boundary condition for the wake origin at the blade(s), the wake solution itself is dependent on the blade flapping solution. Therefore, Eq. 1 must be solved with the wake solution in a properly coupled manner.

The second-order equation describing the blade flapping motion (Eq. 1) can be reduced to a set of first-order ordinary differential equations (ODEs). This set of equations can be solved using various standard integration methods. However, in the present work the proposed second-order backward time-integration algorithm for the wake equations, which is described later in this article, was used to solve these equations. To reduce the equations to first order, the blade flapping equation is rewritten in a matrix form with two variables β and $\dot{\beta}$, i.e.,

$$\frac{d}{d\psi} \begin{Bmatrix} \dot{\beta} \\ \beta \end{Bmatrix} + \begin{bmatrix} v_{\beta}^2 & 0 \\ 0 & 1 \end{bmatrix} \begin{Bmatrix} \dot{\beta} \\ \beta \end{Bmatrix} = \begin{Bmatrix} \frac{M_{\beta}}{I_{\beta} \Omega^2} + \frac{\omega_0^2}{\Omega^2} \beta_p \\ 0 \end{Bmatrix}$$

i.e., $\dot{Y} + [M]Y = f$

or, $\dot{Y} = F(Y(\psi), \psi) \quad (3)$

The stability and accuracy considerations applied to the wake governing equations in the following section also apply to the blade flapping equations written in this generic ODE form (Eq. 3).

Governing Equations of the Rotor Wake

Rotor free-wake methods, like all free-vortex methods, are based on the vorticity transport theorem or Helmholtz second theorem,¹⁹ which states that in a circulation preserving flow (potential flow) vortex lines are material lines. The vorticity is assumed to be concentrated in trailed and/or shed vortex lines in a surrounding potential flow field. In numerical solutions, the vortex lines are discretized into finite vortex elements. The motion of each collocation point of the vortex segments is then given by the Lagrangian equation of motion of a fluid particle, i.e.,

$$\frac{d\vec{r}}{dt} = \vec{V}(\vec{r}) \quad (4)$$

where \vec{r} is the position vector of a collocation point on a vortex segment, and $\vec{V}(\vec{r})$ the local fluid velocity at that point – see Fig. 1. For rotating wing applications, this governing equation may be written in blade fixed coordinates in the form of a partial differential equation (PDE). The blade azimuthal location (ψ) is a temporal coordinate, while the vortex age (ζ) is a spatial coordinate the distance of the vortex element from its origin at the blade tip. Therefore, the vorticity transport equation can be written as

$$\frac{\partial \vec{r}}{\partial \psi} + \frac{\partial \vec{r}}{\partial \zeta} = \frac{\vec{V}(\vec{r})}{\Omega} \quad (5)$$

The left hand side (LHS) of Eq. 5 is the one-dimensional wave (convection) equation. The source term on the right hand side (RHS) is a complicated term because it includes the mutual and self-induced velocities of the vortical wake, as well as relative freestream and maneuver velocities of the rotor/helicopter. To solve Eq. 5 numerically, the derivatives on the LHS are approximated using finite differences. The present work is a development of the method of Bagai & Leishman.¹⁴⁻¹⁶ The approach is to solve the discretized governing equations at the mid-point ($\psi + \Delta\psi/2, \zeta + \Delta\zeta/2$) of a grid cell $[\psi, \psi + \Delta\psi] \times [\zeta, \zeta + \Delta\zeta]$, with the derivatives being approximated by a second-order accurate five-point central difference.

The velocity source term on the RHS of Eq. 5 includes self and mutual induced velocities, which are given by the Biot-Savart law²⁰ as an integral along the length of each vortex filament in the wake. The Biot-Savart integral cannot, in general, be evaluated exactly and must be approximated by numerical quadrature. In the present analysis this integral is evaluated using straight-line vortex segmentation, which is analogous to the trapezoidal rule for numerical quadrature. This approach was found to be second-order accurate for induced velocity calculations – see Ref. 21 for details.

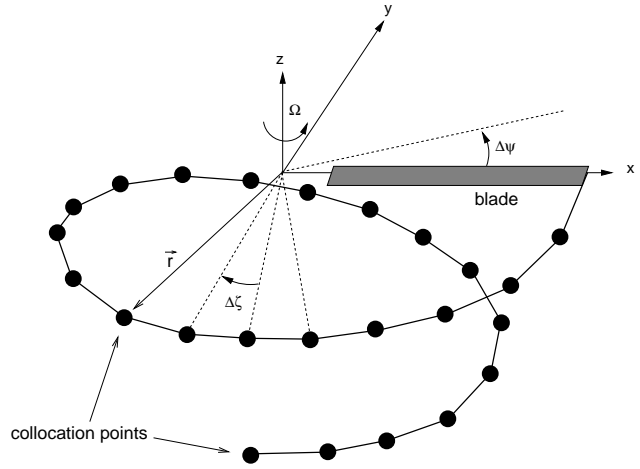


Fig. 1 Schematic of the discretized tip vortex geometry

To enable time-integration of the wake equations, the equations are written again in the form of an ODE, with the wake collocation points \vec{r} as the variables, that is

$$\begin{aligned} \frac{d\vec{r}(\psi, \zeta)}{d\psi} &= \frac{\vec{r}(\psi, \zeta) - \vec{r}(\psi, \zeta + \Delta\zeta)}{\Delta\zeta} + \vec{V}(\vec{r}(\psi, \zeta)) \Big|_{discrete} \\ &= F(\vec{r}(\psi), \psi) \end{aligned} \quad (6)$$

Notice that Eq. 6 is in the same generic ODE form as the blade flapping equation (Eq. 3). Therefore, the same methodology can be applied to solve both sets of governing equations in a fully coupled manner.

In the present work, a new time-marching free-vortex wake algorithm was developed following the basic approach outlined above. This algorithm is referred to as the PC2B (Predictor-Corrector 2nd-Backward) algorithm. Another algorithm, termed as the PCC (Predictor-Corrector Central difference) algorithm, is also used to bring out the importance of stability in convergence of time-marching solutions, in general. In both the PC2B and PCC algorithms, a predictor step is used to obtain a “guess” solution at the new time-step to allow induced velocity calculations in a *pseudo*-implicit manner. A five-point central difference approximation for the spatial (ζ) derivative was used in both algorithms. The key difference between the two new algorithms was the choice of difference approximation for the time (ψ) derivative. The PCC algorithm used a five-point central difference approximation similar to that of Refs. 13–16. The PC2B algorithm used a 2nd-order backward difference approximation as given by

$$\begin{aligned} D_\psi &\approx \frac{\partial \vec{r}(\psi + \Delta\psi/2, \zeta)}{\partial \psi} \\ &= \frac{3\vec{r}(\psi + \Delta\psi, \zeta) - \vec{r}(\psi, \zeta) - 3\vec{r}(\psi - \Delta\psi, \zeta) + \vec{r}(\psi - 2\Delta\psi, \zeta)}{4\Delta\psi} \end{aligned} \quad (7)$$

Linearized Stability Analysis

To analyze the stability of a time-marching algorithm, the algorithm is applied to a representative ordinary differential equation (ODE) of the general form

$$\frac{du}{dt} = \lambda u + a e^{ut} \quad (8)$$

where λ , μ and a are constants. The exact solution to Eq. 8 is given by

$$u(t) = u(0)e^{\lambda t} + a \left(\frac{e^{\mu t} - e^{\lambda t}}{\mu - \lambda} \right) \quad (9)$$

The predictor step in both algorithms is used only for evaluating the induced velocities in a *pseudo*-implicit manner. The spatial differences are, however, calculated in an implicit manner. Therefore, the stability of the time-marching algorithm is determined by the corrector step in the algorithm. The PCC algorithm applied to the above model equation gives

$$u^{n+1} = u^n + \frac{1}{2}\lambda h (u^{n+1} + u^n) + \frac{1}{2}ah (e^{\mu h n} + e^{\mu h(n+1)}) \quad (10)$$

where h is the time step $h = \Delta t = (t^{n+1} - t^n)$. By assuming a solution of the form $u^{n+1} = \sigma u^n$, the eigenvalue(s) of the algorithms can be obtained from

$$\sigma = \frac{1 + \frac{1}{2}\lambda h}{1 - \frac{1}{2}\lambda h} = 1 + \lambda h + \frac{1}{2}\lambda^2 h^2 + \dots + \frac{1}{2^{n-1}}\lambda^n h^n + \dots \quad (11)$$

Similarly, when the PC2B algorithm is applied to the representative equation,

$$3u_{n+1} = u_n + 3u_{n-1} - u_{n-2} + 2\lambda h(u_{n+1} + u_n) + 2ah (e^{\mu h n} + e^{\mu h(n+1)}) \quad (12)$$

and the eigenvalues, σ , are solutions of the characteristic polynomial given by

$$(3 - 2\lambda h)\sigma^3 - (1 + 2\lambda h)\sigma^2 - 3\sigma + 1 = 0 \quad (13)$$

Because for this algorithm the time-integration involves three time-steps, there are three eigenvalues. These are given by

$$\begin{aligned} \sigma_1 &= 1 + \lambda h + \frac{1}{2}\lambda^2 h^2 + \frac{1}{2}\lambda^3 h^3 + \dots \\ \sigma_2 &= \frac{1}{3} - \frac{1}{9}\lambda h + \frac{5}{54}\lambda^2 h^2 + \frac{17}{162}\lambda^3 h^3 + \dots \\ \sigma_3 &= -1 \end{aligned} \quad (14)$$

In this case, only the first eigenvalue or the principal root is important for the accuracy of the solution. The linear stability criterion requires that the amplification factor for each time-step, $|\sigma|$, be less than or equal to unity, that is

$$|\sigma(\lambda = i\omega h)| \leq 1 \quad (15)$$

This implies that the eigenvalues for $\lambda = i\omega h$ must always lie within the unit circle in the complex σ -plane.

To bring out the relative merits of the proposed algorithms, the principal roots for the PCC and PC2B algorithms are shown in Fig. 2 along with results for two other time-marching algorithms that have been previously used for rotor free-wake analyses. The forward Euler algorithm is a one-step explicit method. The Adams-Moulton 4th-order (AM4) algorithm (e.g., see Ref. 22) is also a two-step pseudo-implicit predictor-corrector method, like the PCC

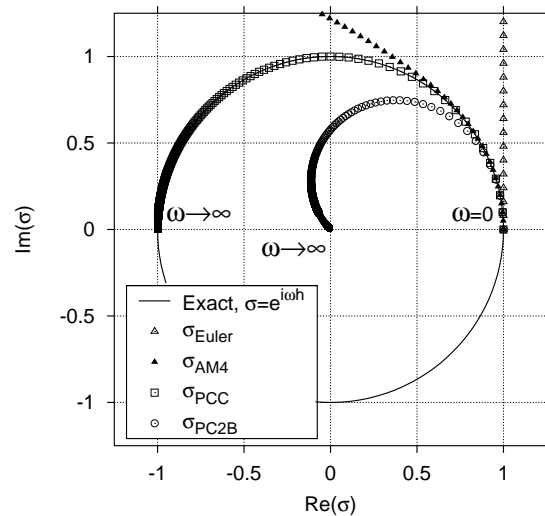


Fig. 2 Principal roots for four time-marching algorithms

and PC2B algorithms. Recall that the stability criterion requires that the σ -eigenvalues lie within the unit circle on the complex σ -plane. The explicit Euler method is clearly unstable because the eigenvalue always lies outside the unit circle. The AM4 algorithm is relatively more stable with the principal σ -root closely following the unit circle for small values of ωh . The PCC algorithm is stable but with no damping, as mentioned previously, whereas the PC2B algorithm is stable with positive damping. It should be noted that the AM4 algorithm is formally 4th-order accurate, and for very small values of ωh it is only mildly unstable. However, for practical applications of the free-wake in helicopter analyses, which will have typical time-steps of $\Delta\psi = 5^\circ$ to 15° , this algorithm will be unsuitable because even though it has a better order of accuracy it is still unstable.

Nonlinear Stability Considerations

It must be noted that the stability analysis of time-marching algorithms in the preceding section is strictly applicable only to linear equations. For nonlinear equations, the numerical solution may exhibit spurious oscillations, albeit these may remain bounded for a given discretization level. This implies that the solution is stable in a linear sense, however, it may not be convergent because of the grid-dependent spurious numerical oscillations. Therefore, to ensure stability of nonlinear equations a broader definition of stability must be considered. Following the philosophy of traditional CFD analyses, a given numerical algorithm may be considered to be unstable if the numerical errors start out small and grow with time.²³ The linearized stability condition is just a special case of this broader consideration and should be used only as a necessary guideline for the non-linear equations.

To better understand this concept of stability, free-vortex wake solutions using the two algorithms are shown in

Fig. 3. The rotor geometry and operating conditions correspond to those reported in Ref. 10. The initial condition for both time-integration algorithms was obtained using a steady-state (relaxation based) free-vortex wake model. The solutions are shown after fifteen rotor revolutions (i.e., at $\psi_b = 30\pi$), along with the initial wake geometry. The PCC solution, as shown in Fig. 3(a), indicates the presence of numerical errors in the form of sinusoidal disturbances. The initial condition did not contain such disturbances and, therefore, these disturbances are purely numerical in origin. The PC2B solution, however, shows no such disturbances – see Fig. 3(b). Therefore, following the broader sense of nonlinear stability, the PCC algorithm is unstable while the PC2B algorithm is stable and, therefore, only this algorithm would lead to a properly converged wake solution.

Results and Discussion

Convergence of Wake Solution

A numerical experiment was performed to verify the convergence of free-vortex wake solution with increasing grid refinement, i.e., with a finer azimuth step and increased wake resolution. This numerical experiment verified that the final wake solution is second-order accurate in ψ and ζ , as expected from the preceding analysis. Also, because stability and consistency of the numerical method are necessary for solution convergence, such numerical experiments can also verify the stability of the numerical algorithms. It was shown that both the PCC and the PC2B algorithms are consistent with the original governing equations. Therefore, convergence of the wake solution can be used as a test to establish the stability of the numerical algorithms.

A grid resolution study with the free-vortex wake was performed using both the PCC and PC2B time-marching algorithms, with discretization levels ranging from $\Delta\psi = \Delta\zeta = 2.5^\circ$ to 20° . Although the exact (mathematical) solution for the wake geometry is forever unknown, the numerical solution with the finest grid discretization can be considered as the “exact” solution for the purposes of estimating the order of accuracy. Numerical errors were calculated relative to this wake geometry using the finest grid ($\Delta\psi = \Delta\zeta = 2.5^\circ$).

Figure 4 shows the numerical errors in the wake geometry as a function of grid discretization level. Because the solution is expected to show second-order accuracy, quadratic fits to the numerical results are also shown. These results confirm that the final wake geometry solution obtained using the PC2B algorithm is, indeed, second-order accurate in both space (ζ) and time (ψ).

Finally, the numerical experiment was repeated for a forward flight case at an advance ratio $\mu = 0.1$ to verify wake solution convergence. At this advance ratio the mutually induced effects from the tip vortices generated by each blade are relatively powerful, and significant wake distortion is to be expected. The calculations were performed for a four-bladed rotor whose geometry and operating conditions correspond to the experiments of Ref. 24. A forward shaft tilt angle of -3° was used with a rotor thrust coef-

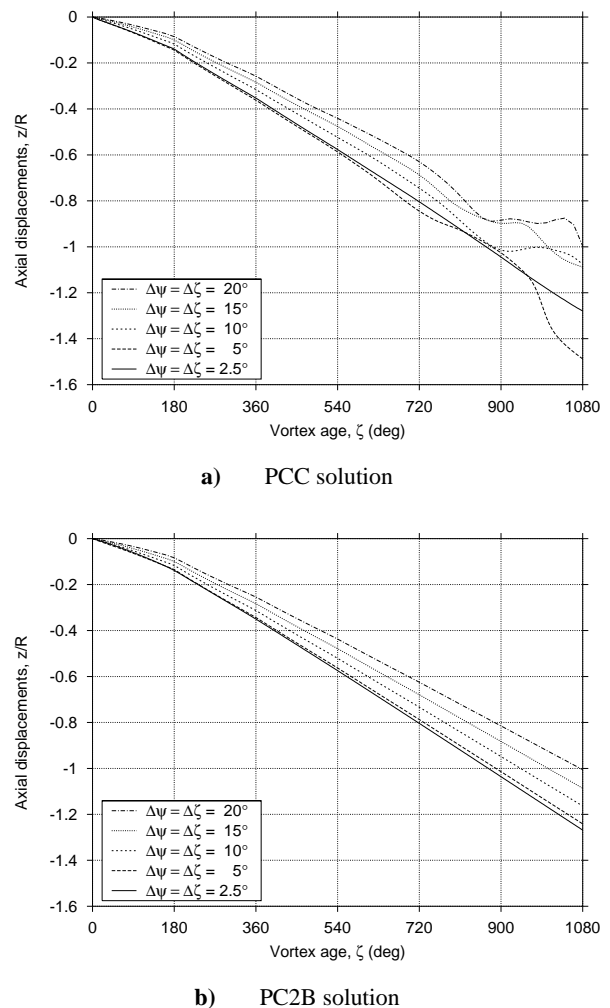


Fig. 3 Sample results for free-vortex wake calculations using (a) PCC algorithm, and (b) PC2B algorithm, for a two-bladed hovering rotor showing axial displacements of the tip vortex from the reference blade (blade 1)

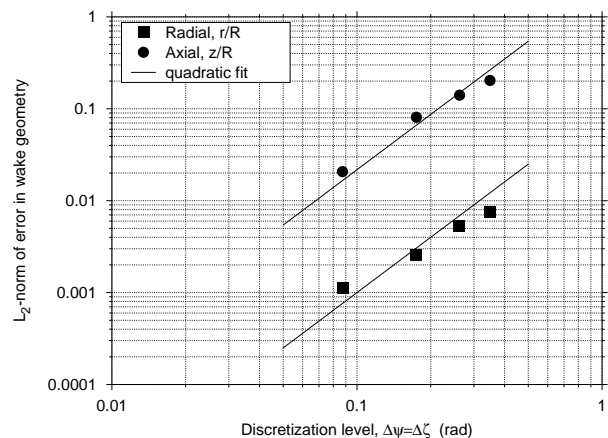


Fig. 4 Numerical errors in free-vortex wake solution using the PC2B algorithm in hover with increasing grid discretization. Quadratic decreasing trend indicates a second-order accuracy

efficient of $C_T = 0.008$. The top (plan) and side views of the rotor wake geometry are shown in Fig. 5(a) and 5(b) for different levels of discretization. Only the geometry for tip vortex from a reference blade at $\psi_b = 0^\circ$ is shown for clarity. Notice that only the solution with the coarser discretization of $\Delta\psi = \Delta\zeta = 20^\circ$ shows significant differences from the other solutions. The solutions corresponding to $\Delta\psi \leq 10^\circ$ are almost identical. The numerical errors, relative to the $\Delta\psi = 2.5^\circ$ solution, exhibit the expected second-order accuracy, as shown in Fig. 5(c).

Therefore, it can be concluded from these numerical experiments that the PC2B solution is convergent in both hover and forward flight. It is particularly significant to note that the strong distortions present in the wake structures are well-preserved, and not damped-out because of the artificial numerical dissipation.

Maneuvering Rotors: Change in Collective Pitch

The time-accurate free-wake model based on the PC2B algorithm was applied to solve for the transient rotor wake dynamics and rotor flapping response following an elementary maneuver in the form of a ramp (constant pitch rate) increase in the collective pitch of the rotor blades.

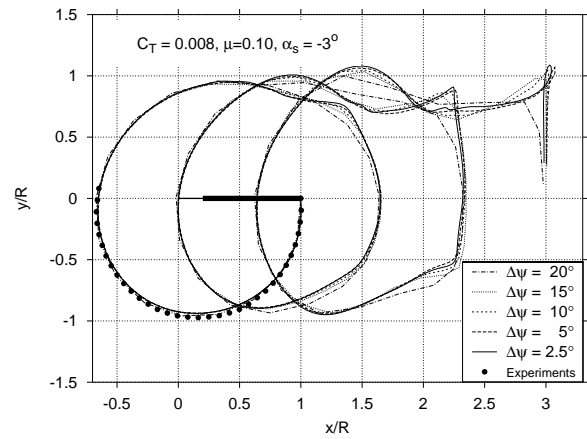
To initially validate the time-accurate free-wake methodology, the response of a three-bladed articulated rotor to a change collective pitch was examined. This is a classic problem that was experimentally examined by Carpenter & Friedovich²⁵ for a full-scale isolated rotor. The rotor blades had a radius of 5.8 m (19 ft) and a solidity of 0.042. The rotor was operated at approximately 220 rpm. In the experiments, the collective pitch of the blades was increased linearly at different constant rates to a maximum pitch of 12 degrees. The blade flapping angles, rotor thrust and mean rotor inflow were measured in the experiment.

Figure 6 shows the results for the highest ramp rate of 200 degrees per second along with the experimental measurements. Notice that the collective input in the experiments shows some oscillatory overshoot behavior, which is because of blade torsion. The rotor thrust and flapping show significant initial overshoots compared to their steady-state values, both of which are attributable to the lag in the development of the inflow. The relatively slow build-up of the mean rotor inflow observed in the experiments has been previously attributed to the apparent mass (i.e., the non-circulatory or inertial effects) of the fluid surrounding the rotor disk, although it will be shown later in this article that this lag is predominantly a circulatory effect.

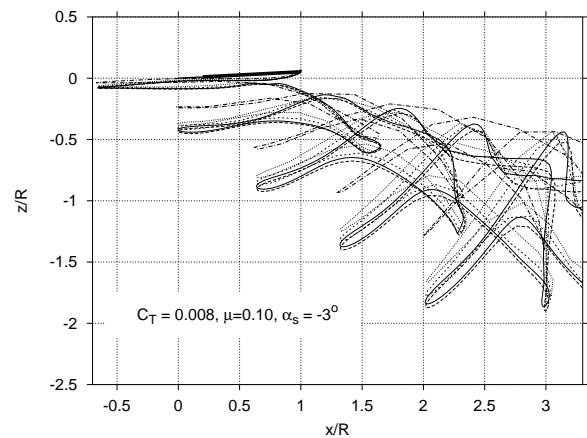
Dynamic Inflow Equation

Under the assumption of uniform inflow over the rotor disk, an equation for dynamic (time-dependent) inflow can be obtained by equating rotor thrust obtained using a blade-element theory and annular momentum theory – see Ref. 25 for details. The rotor thrust is given by

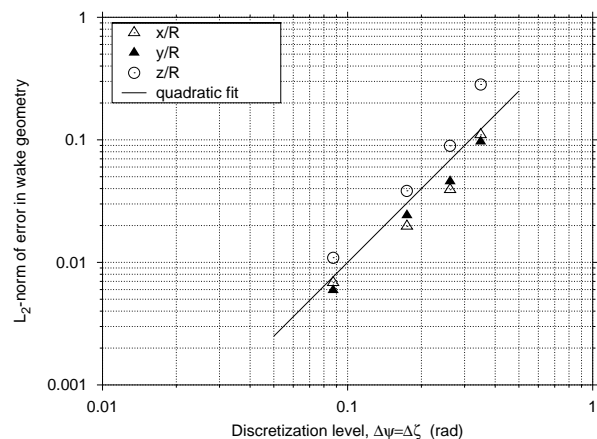
$$T = m_a \dot{v}_i + 2\pi R^2 \rho v_i \left(v_i + \frac{2}{3} \dot{\beta} R \right)$$



a) Top view of tip vortex geometry



b) Side view of tip vortex geometry



c) Convergence trend

Fig. 5 The PC2B algorithm applied to free-vortex wake geometry solution in forward flight: (a) side view of tip vortex geometry (b) numerical errors with increasing grid discretization showing convergence

$$= \frac{1}{6} N_b \rho c C_{l\alpha} \Omega^2 R^3 \left(\theta - \frac{3}{2} \frac{v_i}{\Omega R} - \frac{\dot{\beta}}{\Omega} \right) \quad (16)$$

where m_a is the apparent mass of a solid circular disk.²⁶ The $m_a \dot{v}_i$ term, therefore, is meant to represent the additional force on the rotor disk because of the accelerating inflow. The analogy drawn between a fluid accelerating through a permeable disk and a solid circular disk accelerating in a stagnant fluid is not rigorous. However, proceeding on this basis the dynamic inflow equation is given by

$$m_a \dot{v}_i = 2\pi R^2 \rho v_i \left(v_i + \frac{2}{3} \dot{\beta} R \right) + \frac{1}{6} N_b \rho c C_{l\alpha} \Omega^2 R^3 \left(\theta - \frac{3}{2} \frac{v_i}{\Omega R} - \frac{\dot{\beta}}{\Omega} \right) \quad (17)$$

Note that in the above derivation the inflow is assumed to be uniform over the blade span. Therefore, a simple correction factor is included to account for non-uniform inflow – see Ref. 25 for details. This equation is then solved together with the blade flapping equations of motion.

Comparison with Experiments

The results using this dynamic inflow model are shown in Fig. 6 along in with the free-vortex wake results. In this case, the blade flapping dynamics were fully coupled with the wake solution during every time-step. The transient free-vortex wake results were obtained using an initial wake geometry corresponding to a very small thrust coefficient. The initial mean inflow and coning angle were also negligibly small. The wake geometry and the blade flapping response were then calculated in a coupled manner by time-integrating the respective equations.

Figure 6 shows that the rotor thrust response and inflow build-up is in good agreement with experimental measurements. The transient overshoot in flapping (coning) is slightly underpredicted because the participation of the torsional blade dynamics, albeit small, have been neglected in the analysis. The slow build-up of inflow, which is modeled basically as a time-lag in the dynamic inflow theory, is a result of the transient evolution of the trailed rotor wake. This time constant (lag) of the dynamic inflow build-up can be estimated using the linear portion of Eq. 17 in a non-dimensional form, i.e.,

$$0.85 \lambda_i^* = -\frac{1}{4} \sigma C_{l\alpha} \lambda_i$$

i.e., $\frac{0.85 \times 4}{\sigma C_{l\alpha}} \lambda_i^* = -\lambda_i \quad (18)$

Now, assuming $C_{l\alpha} = 2\pi/\text{rad}$ the inflow time constant can be identified as

$$\tau = \frac{0.541}{\sigma} \text{ radians} = \frac{0.541}{2\pi\sigma} \text{ rotor revolutions} \quad (19)$$

Therefore, for Carpenter & Friedovich's rotor experiment the time constant for the unsteady flow development is approximately two rotor revolutions, which is relatively long.

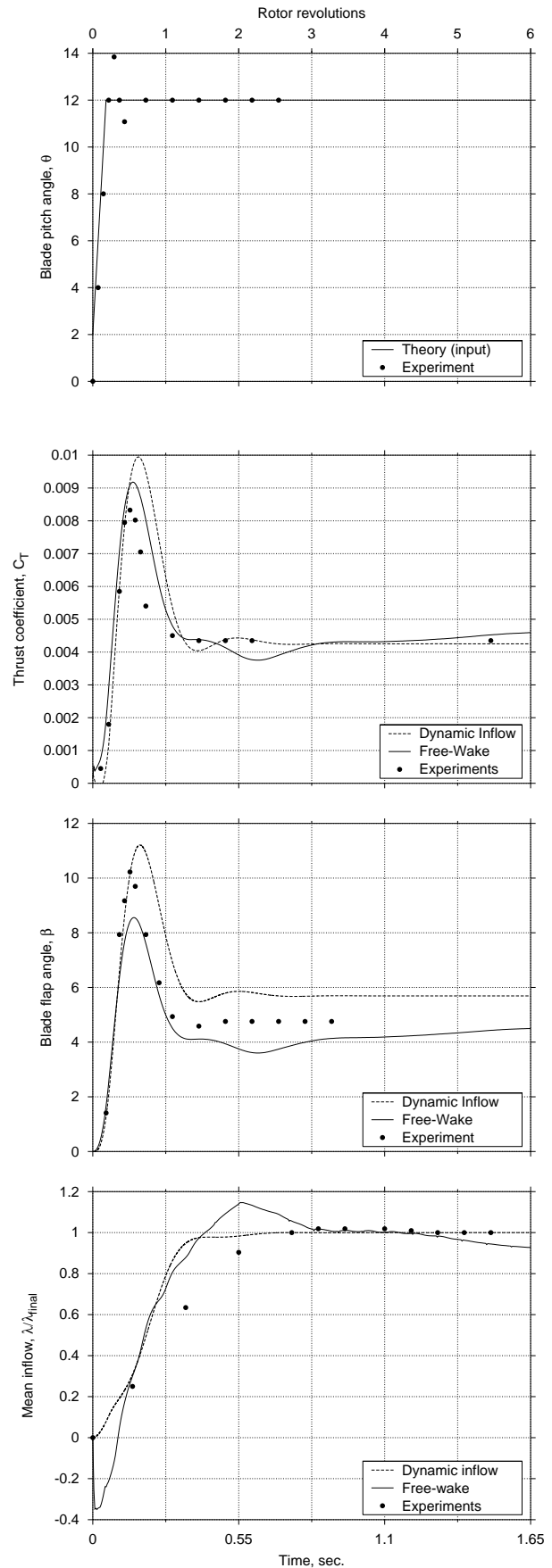
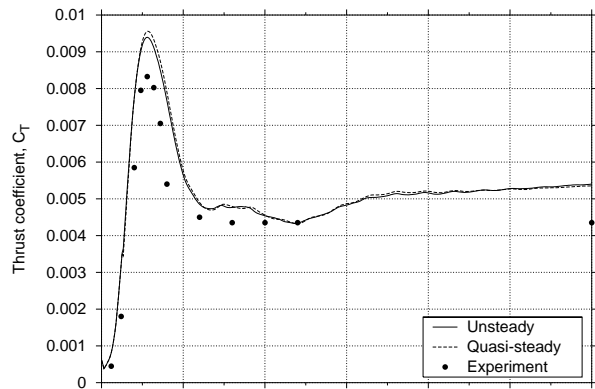
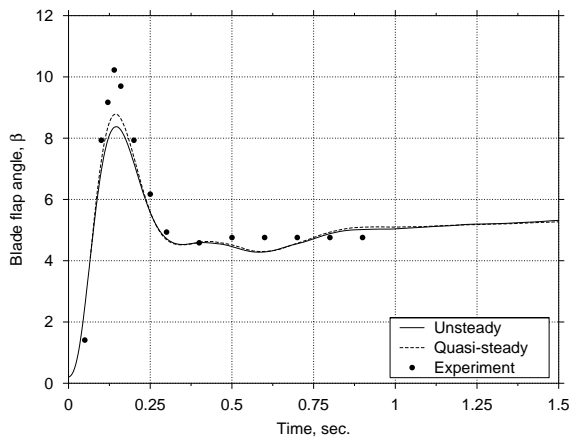


Fig. 6 Rotor response following a ramp increase in rotor collective pitch angle at the rate of 200 deg/sec. Three-bladed articulated rotor in hover. Experimental results from Ref. 25



a) Rotor thrust



b) Blade flapping angle

Fig. 7 Effect of unsteady aerodynamic effects on the rotor response following a ramp increase in collective pitch at 200 deg/sec. Experimental results from Ref. 25

Note that this time-constant is correctly predicted by the time-accurate wake algorithm, as shown in Fig. 6. Good correlations were also obtained for other ramp rates examined in the experiments.

Role of Unsteady Aerodynamic Effects

The apparent mass term that appears in the dynamic inflow model described above, appears to suggest unsteady aerodynamic lift increments. Therefore, the role of the apparent mass terms in this transient rotor response has been examined. To do this, the non-circulatory unsteady aerodynamic terms corresponding to the apparent mass effects at each blade-element (e.g., Ref. 18) were included in the blade lift solution. These results are shown in Fig. 7 for the 200 degree per second ramp rate. Again, notice that these unsteady aerodynamic effects are found to be much smaller compared to the overall rotor response. The rotor thrust and blade flapping overshoots observed in this maneuver are, therefore, a result mostly of the transients associated with trailed wake evolution, i.e., a circulatory effect. The development of the rotor wake following the collective pitch

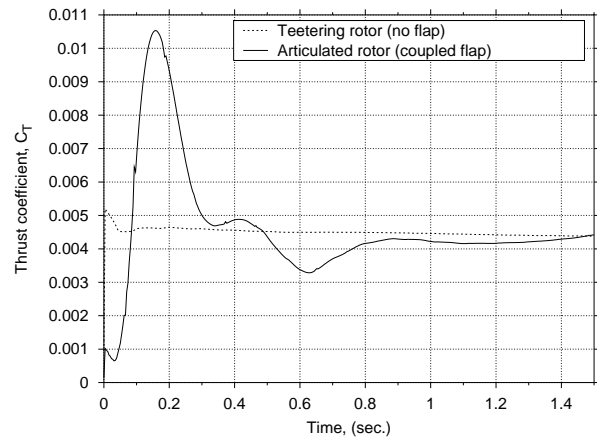


Fig. 8 Effect of coupled blade flapping dynamics on the transient rotor response

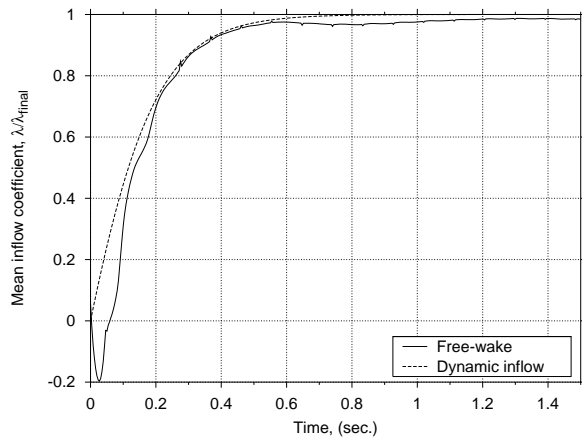
change results in a relatively slow build-up of the inflow induced through the rotor disk, thereby leading to a transient overshoot in rotor thrust.

Effects of Flap Dynamics

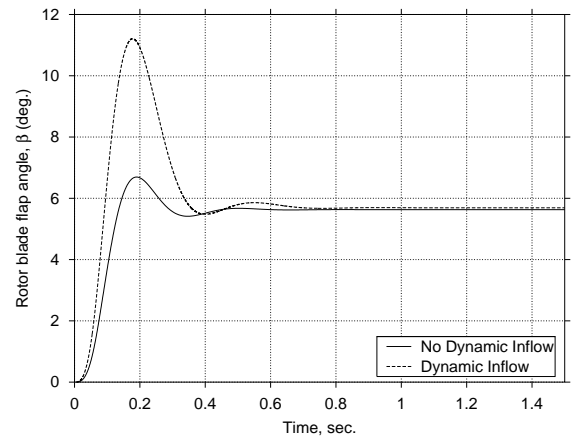
The above results show the influence of the inflow dynamics induced by the trailed vortex system alone. For the teetering rotor in hovering or axial flight there is no blade flapping because of wake axisymmetry. Typically, blade flapping dynamics will augment the transient overshoot in rotor thrust. This is because following an increase in collective there will be a transient overshoot in blade flapping, which will move the rotor blades further away above the trailed wake. This results in a further delay in build-up of rotor inflow and a corresponding larger thrust overshoot.

Figure 8 shows results for a rigid (non-flapping) rotor and an articulated rotor to bring out the inherent coupling between the blade flapping motion and the rotor wake dynamics. Notice that the articulated rotor shows a substantially higher transient rotor overshoot compared to the teetering rotor. Clearly, the overall response of the rotor to such inputs is strongly dependent on both the rotor wake dynamics as well as the blade flapping dynamics.

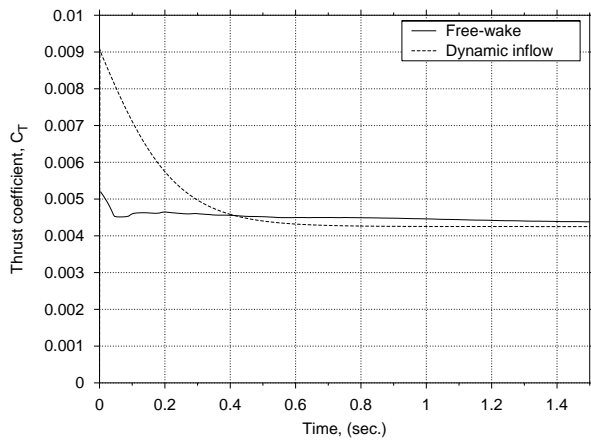
Another numerical experiment was performed to examine the relative effects of the inflow dynamics and blade flapping dynamics. Recall that the dynamic inflow model showed essentially the same inflow response as the free-vortex wake model. Therefore, only the relative effects of dynamic inflow and blade flapping were examined. Figure 9 shows the build-up of rotor inflow and the thrust coefficient as a function of time following a step increase in collective pitch. The rotor geometry is identical to the experiments of Carpenter & Friedovitch,²⁵ but in this case the rotor was assumed to be gimbaled and, therefore, there was no blade flapping. Notice that the predicted inflow build-up is nearly the same using both the dynamic inflow and the free-wake models. The rotor thrust, however, is substantially overpredicted with the dynamic inflow model. This suggests that the dynamic inflow theory is limited in ap-



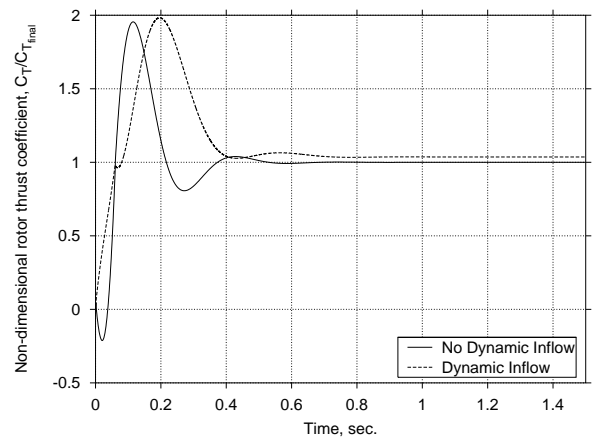
a) Blade flapping angle



a) Blade flapping angle



b) Rotor thrust response



b) Rotor thrust response

Fig. 9 The relative effect of blade flapping dynamics in transient rotor response (a) blade flapping angle, (b) rotor thrust following a ramp increase in rotor collective pitch.

Fig. 10 The relative effect of wake/inflow dynamics in transient rotor response (a) blade flapping angle, (b) rotor thrust following a ramp increase in rotor collective pitch.

plication to specific rotor configurations, unless empirical corrections to the dynamic inflow coefficients are used.

Figure 10 shows the results for the Carpenter & Friedovitch rotor obtained using the dynamic inflow theory along with results obtained by eliminating the inflow dynamics. In this case, following a simple blade element/momentum theory (i.e., ignoring the time-dependent terms in Eq. 17), the inflow is proportional to the collective pitch input. The blade flapping results, as shown in Fig. 10(a), bring out the importance of inflow dynamics in the blade flapping motion. Clearly, the results obtained by ignoring time-varying rotor inflow significantly underpredict the blade flapping. However, it is interesting to note that the overshoot in the thrust with a constant inflow is the same as that obtained using dynamic inflow. Therefore, the blade flapping dynamics certainly plays a dominant in transient rotor response. However, there is an increased lag in thrust overshoot, which is correctly modeled with the dynamic inflow models.

Frequency Response: Oscillatory Collective Pitch Inputs

The dynamic response of the rotor wake to a step or ramp change in the collective pitch can be idealized a combination of responses to a series of inputs at several different frequencies. In this section, the behavior of the wake-induced rotor inflow over a range of excitation frequencies is examined. This behavior has been experimentally examined in the past to provide some empirical insights into the formulation of dynamic inflow models. The rotor wake dynamic response at low and intermediate range of frequencies below the rotational frequency is also of particular interest from the perspective of helicopter flight dynamics and handling qualities.

The experimental results presented in this section are from the work of Ellenrieder & Brinson.²⁷ In these experiments, a small-scale, four-bladed rotor with rectangular planform, untwisted blades was used. The rotor radius was 0.77 m, the chord was 0.06 m, and the rotor was operated at a nominal rotational speed of 1200 rpm ($125.66 \text{ rad s}^{-1}$).

The rotor blades were mounted on a hub without any blade flapping or lag hinges, resulting in a very stiff rotor with an equivalent flapping hinge offset of $e = 25\%R$. The measured non-dimensional flapping frequency of the rotor, v_β , was found to be 1.22, with a control phase lag angle of 55° in hover. The rotor was operated at a nominal thrust of 280 N or at a thrust coefficient of 0.013. The blade pitch inputs for both collective and cyclic excitations consisted of root pitch changes of 1.5° in magnitude.

The collective pitch excitation was accomplished by changing the pitch settings of all four blades exactly in phase. The inflow time-history showed a small initial transient, after which the predominant response was found to be at the excitation frequency. A frequency analysis was then performed on the time-history to find the amplitude and phase of the inflow response. These inflow frequency responses are shown in Fig. 11 as a function of the excitation frequency and at three representative radial locations at (a) $r/R = 0.41$, (b) $r/R = 0.57$, and (c) $r/R = 0.73$, respectively. The free vortex wake results are shown as solid lines while the corresponding experimental measurements of Ellenrieder & Brinson²⁷ are shown with open symbols.

An interesting feature of these results is the relatively flat gain slope observed at low frequencies, followed by a decrease in gain at half the rotational frequency, and a subsequent gain recovery near the natural frequency of blade flapping (1.22Ω). The present time-accurate free-vortex wake methodology predicts these features correctly. The magnitude of the gains, however, is somewhat under-predicted at low frequencies and over-predicted at higher frequencies. The discrepancies may be because of several reasons, including the fact that experimental measurements were not made at the rotor plane but at a small distance below to avoid risk of sensor contact with the rotor. However, the overall agreement between predictions and experiments is good. In particular, the phase angles of the inflow response are predicted well by the present free-wake analysis. The low phase lag at frequencies lower than the blade flapping natural frequency is an interesting result. Most commonly used dynamic inflow models use empirical values to model this behavior, whereas the present analysis predicts the behavior from first principles.

Figure 12 shows the gain of the dynamic inflow response along the span of the blade in response to a collective pitch excitation. Clearly, the frequency response shows significant variations with both excitation frequency and the radial location. For low excitation frequencies, the inflow response is nominally constant over the blade span. However, as the excitation frequency increases, the inflow response becomes concentrated near the tip region at about $r/R = 0.8$. This trend is also observed in the experiments of Ref. 27. This is an interesting observation because the maximum inflow response approximately corresponds to the spanwise location of the maximum in blade lift.

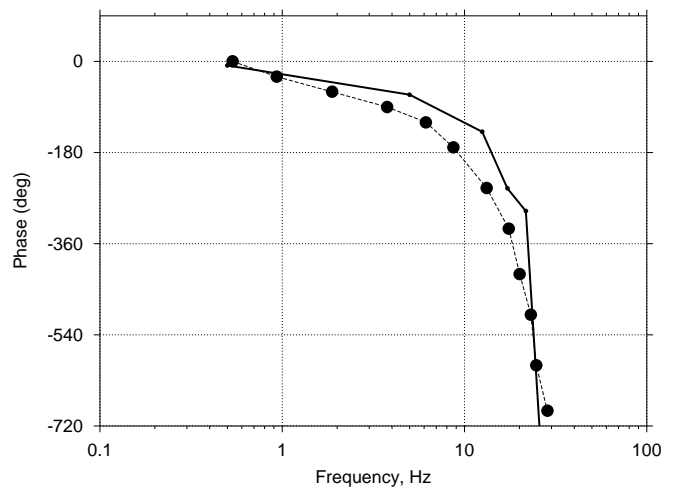
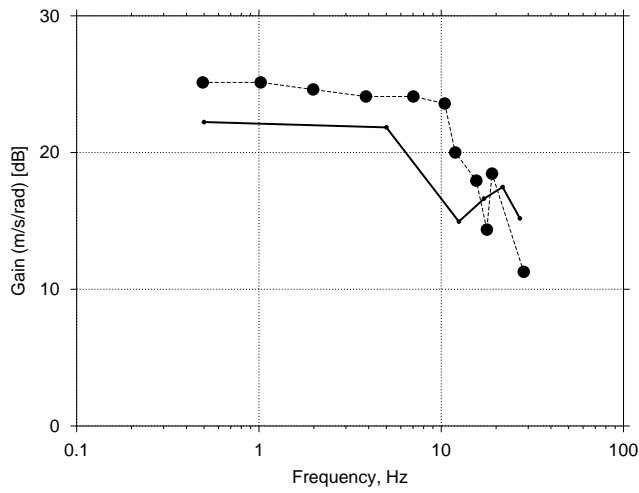
The corresponding phase of the inflow response along the blade span is shown in Fig. 13. At low frequencies, the inflow is essentially in phase with the collective pitch exci-

tion. As the excitation frequency is increased, the phase lag increases over the inboard portion of the blades. This trend is observed in the experiments and is well modeled by the free-vortex wake analysis. Ellenrieder & Brinson have postulated that the increasing phase lag over the inboard sections of the blade is suggestive of the fact that the trailing vorticity from the blade tips is the most dominant flow structure. This observation is confirmed by the present analysis. The good agreement with experimental measurements confirms the inherent assumption that the blade tip vortices are the most dominant flow structure in a rotor wake and dominates both the steady-state and the dynamics of the rotor inflow response.

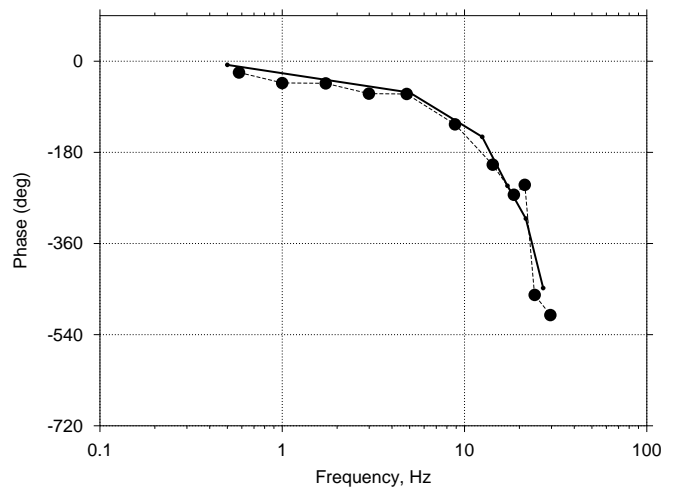
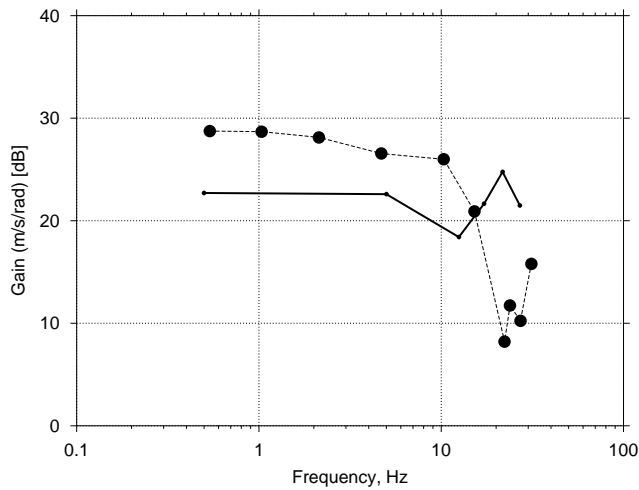
Conclusions

A time-accurate free-vortex wake algorithm has been developed for the calculation of rotor wake dynamics under transient conditions. The choice of the algorithm was based on stability considerations to ensure solution convergence. It was shown that because the governing equations of the rotor wake are highly nonlinear, a linear stability analysis alone is insufficient to guarantee a convergent algorithm. The proposed time-integration algorithm was shown to be convergent with grid refinement and solution convergence was demonstrated with a clean second-order accuracy. The transient rotor response following a ramp increase in rotor collective pitch, as well as the response to oscillatory collective pitch inputs, showed good agreement with experimental measurements. The conclusions drawn from this study are summarized as follows:

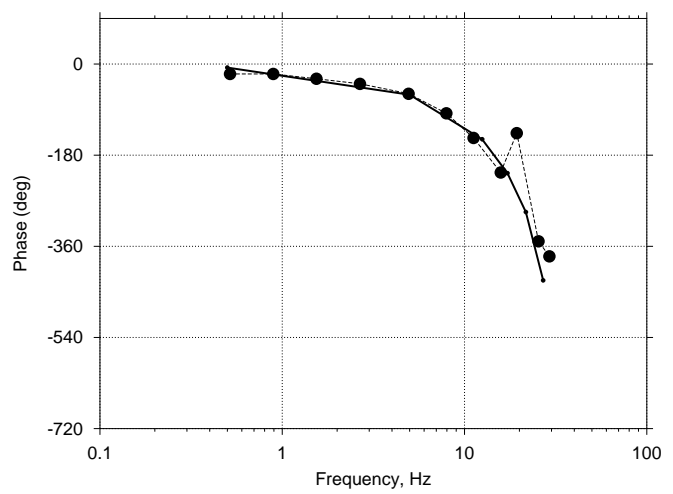
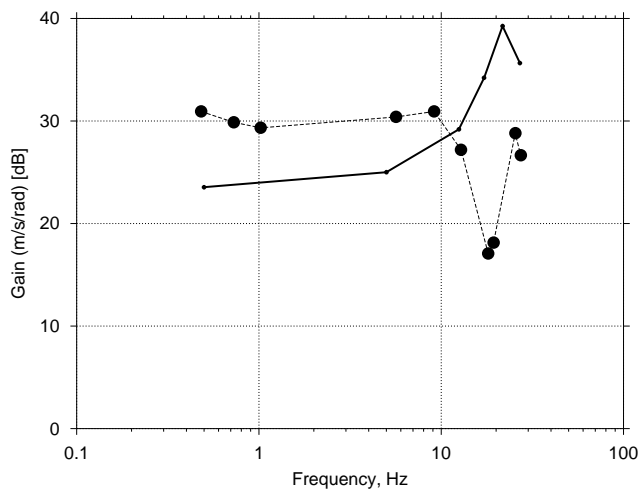
1. Two second-order accurate algorithms (the PCC and PC2B algorithms) were examined for stability and convergence. Both the algorithms were shown to be stable based on a linearized analysis. However, the PCC algorithm (which is based on central differences) must be considered unstable in the sense that it results in growth of numerical errors with time. The PC2B algorithm (which is based on 2nd-order backward differences) contains some inherent dissipation, which effectively restricts the growth of such numerical errors and is the method of choice.
2. The PC2B algorithm was shown to exhibit solution convergence with a clean second-order accuracy. For finer discretizations, such as with an azimuthal step size of 5° or smaller, the solution was shown to be grid-independent. This confirms that the PC2B algorithm is stable, consistent and convergent. This makes the algorithm suitable for the numerical modeling of time-accurate rotor wake dynamics.
3. The time-accurate wake model was shown to give good predictions of the rotor response following a ramp increase in rotor collective pitch. The rotor response in this case was found to be dominated by the dynamic evolution of the trailed wake (tip vortex) system and not the unsteady effects associated with the shed wake or apparent mass (flow inertia effects).



a) At radial location $r/R = 43\%$

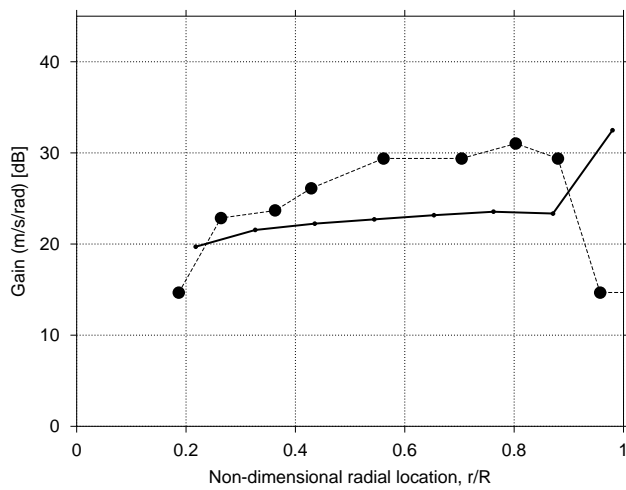


b) At radial location $r/R = 55\%$

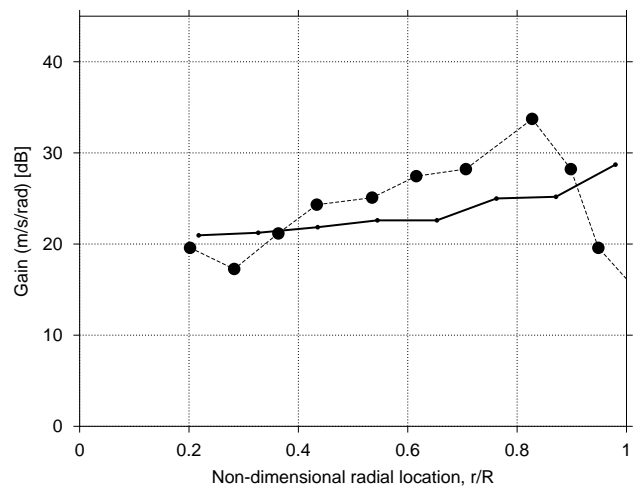


c) At radial location $r/R = 76\%$

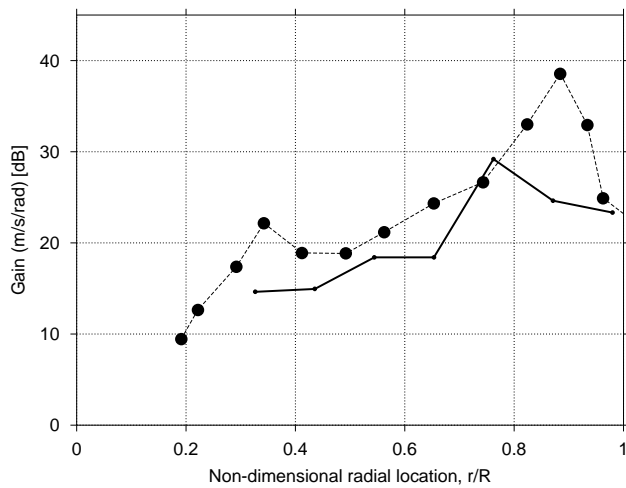
Fig. 11 Magnitude and phase of the inflow frequency response to cyclic excitation of collective pitch. Solid symbols are experimental measurements of Ref. 27 while solid lines are free-vortex wake predictions.



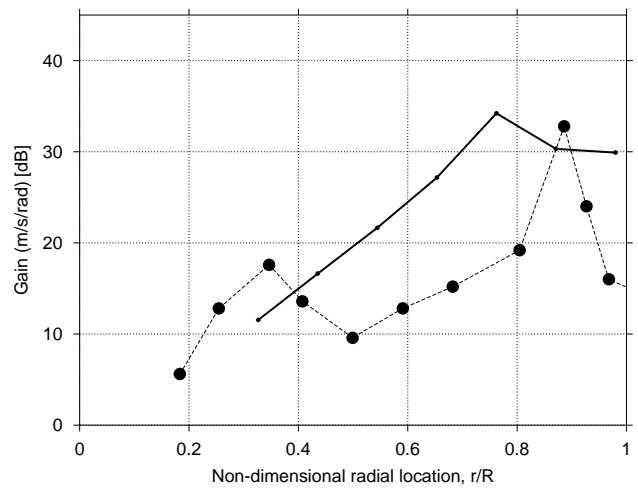
a) 0.5 Hz



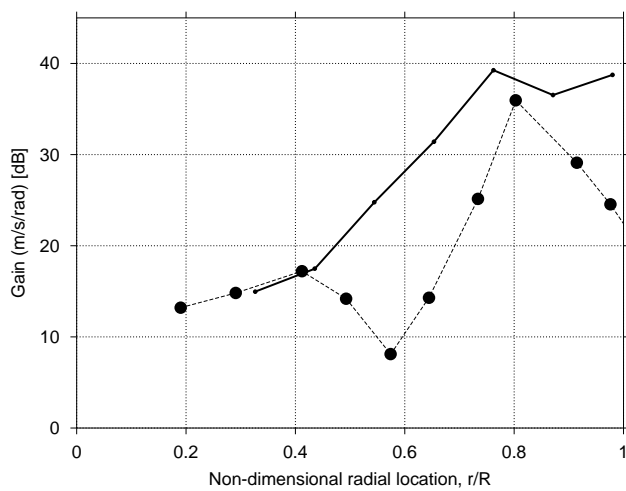
b) 5.0 Hz



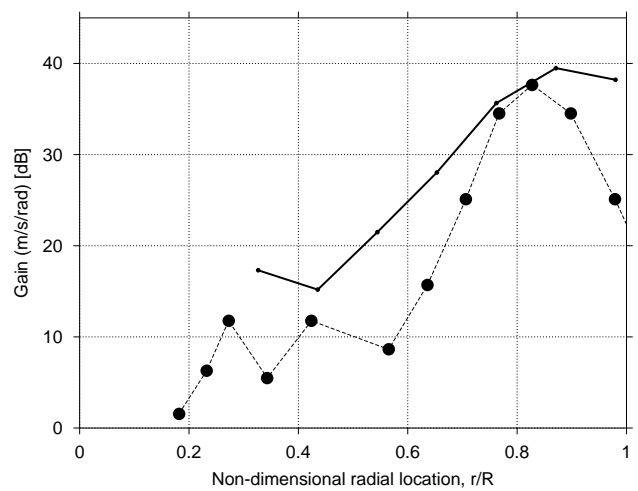
c) 12.5 Hz



d) 17.2 Hz

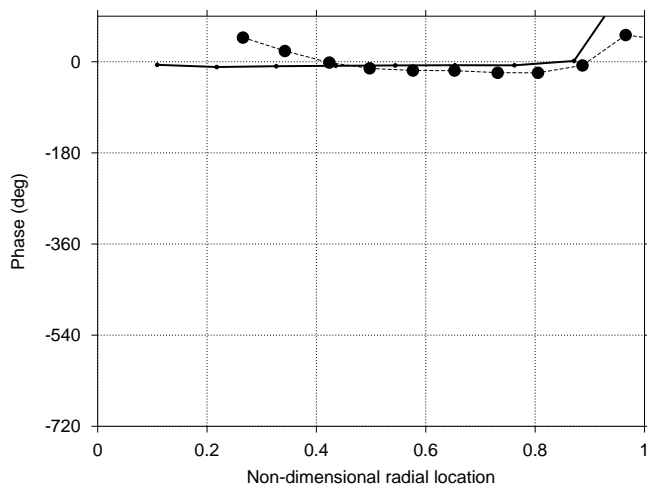


e) 21.7 Hz

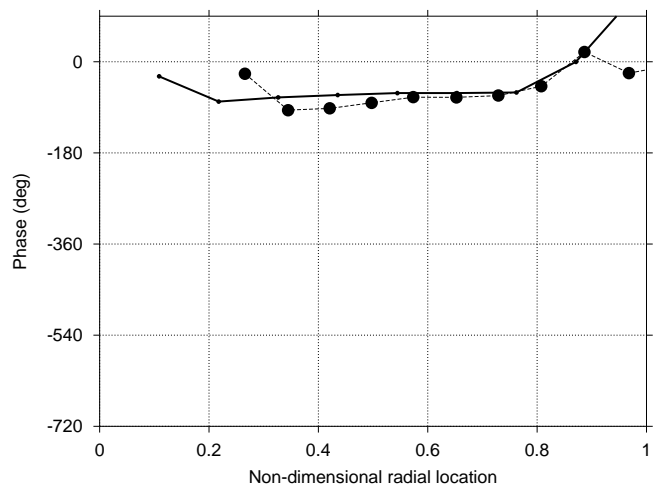


f) 27.0 Hz

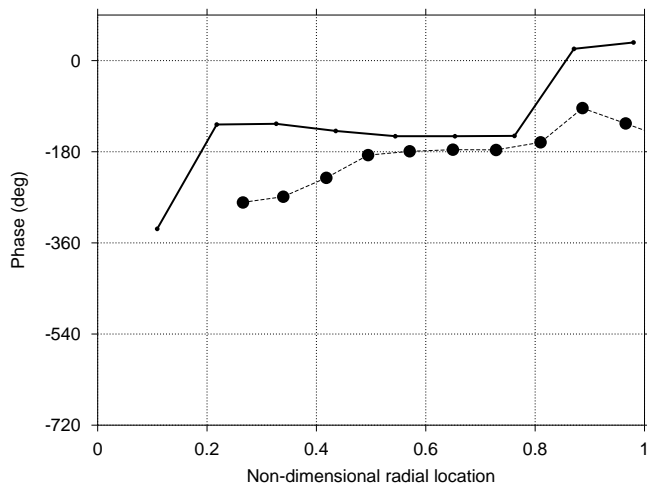
Fig. 12 Radial variation in the gain of dynamic inflow response for different frequencies. Solid symbols are experimental measurements of Ref. 27 while solid lines are free-vortex wake predictions.



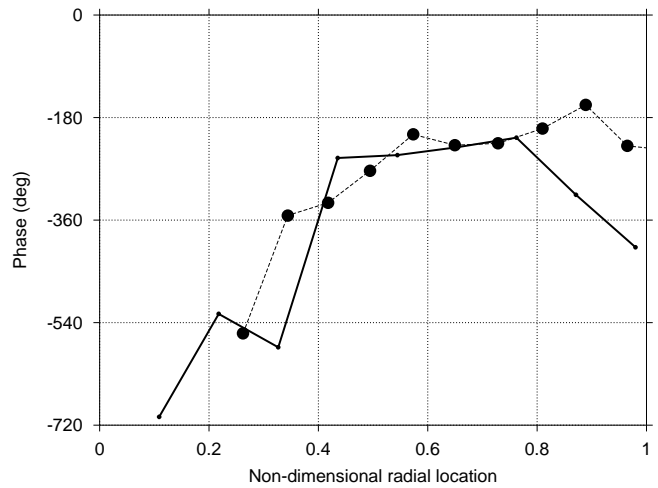
a) 0.5 Hz



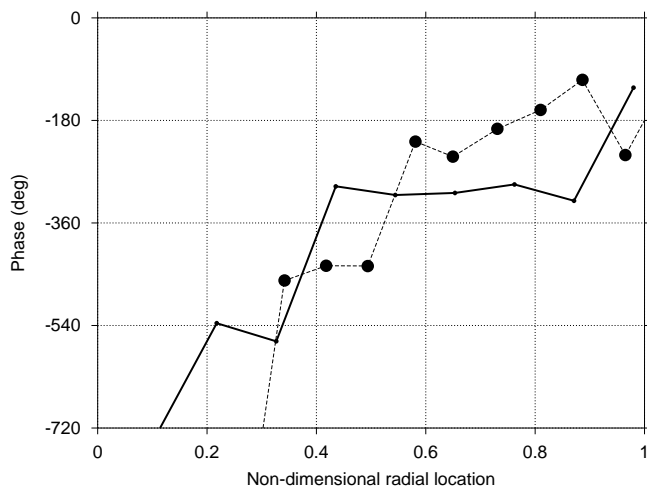
b) 5.0 Hz



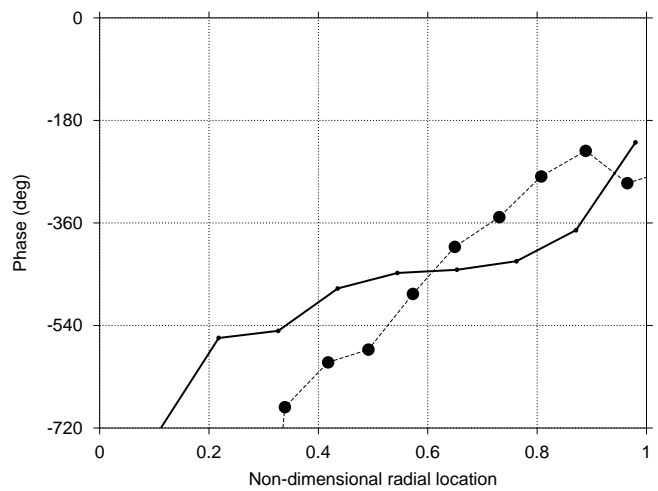
c) 12.5 Hz



d) 17.2 Hz



e) 21.7 Hz



f) 27.0 Hz

Fig. 13 Radial variation in the phase of dynamic inflow response for different frequencies. Solid symbols are experimental measurements of Ref. 27 while solid lines are free-vortex wake predictions.

4. The methodology was applied to solve for the dynamic rotor response to oscillatory collective pitch inputs. An interesting feature of the results was the relatively flat gain slope observed at low frequencies, followed by a decrease in gain at half the rotational frequency and a subsequent gain recovery near the natural frequency of blade flapping. The predicted results for the inflow gain and phase at all excitation frequencies were found to be in good agreement with the corresponding experimental measurements.

Acknowledgments

This work was supported by the National Rotorcraft Technology Center under grant NCC 2944.

References

¹Leishman, J. G. and Bagai, A., "Challenges in Understanding the Vortex Dynamics of Helicopter Rotor Wakes," *AIAA Journal*, Vol. 36, No. 7, July 1998, pp. 1130–1140.

²Theodore, C. and Celi, R., "Flight Dynamic Simulation of Hingeless Rotor Helicopters Including a Maneuvering Free Wake Model," *Proceedings of the 54th Annual American Helicopter Society Forum*, Washington, DC, May 1998.

³Bagai, A., Leishman, J. G., and Park, J., "Aerodynamic Analysis of a Helicopter in Steady Maneuvering Flight Using a Free-Vortex Rotor Wake Model," *Journal of the American Helicopter Society*, Vol. 44, No. 2, April 1999, pp. 109–120.

⁴Quackenbush, T. R., Keller, J. D., Wachspress, D. A., and Boschitsch, A. H., "Reduced Order Free Wake Modeling for Near Real Time Simulation of Rotorcraft Flight Mechanics," *Proceedings of the 55th Annual American Helicopter Society Forum*, Montréal, QC, May 1999.

⁵Crimi, P., "Theoretical Prediction of the Flow in the Wake of a Helicopter Rotor," Tech. Rep. Report BB-1994-5-1, Cornell Aeronautical Laboratory, Buffalo NY, September 1965.

⁶Quackenbush, T. R., Bliss, D. B., and Wachspress, D. A., "Computational Analysis of Hover Performance using a New Free Wake Method," *Proceedings of the 2nd International Conference on Rotorcraft Basis Research*, College Park, MD, February 1988.

⁷Johnson, W., "A General Free Wake Geometry Calculation For Wings and Rotors," *Proceedings of the 51st Annual American Helicopter Society Forum*, Fort Worth, TX, May 1995.

⁸Landgrebe, A. J., "The Wake Geometry of a Hovering Rotor and its Influence on Rotor Performance," *Journal of the American Helicopter Society*, Vol. 17, No. 4, October 1972, pp. 2–15.

⁹Tangler, J. L., Wohlfeld, R. M., and Miley, S. J., "An Experimental Investigation of Vortex Stability, Tip Shapes, Compressibility, and Noise for Hovering Model Rotors," Tech. Rep. CR-2305, NASA, September 1973.

¹⁰Martin, P. B., Bhagwat, M. J., and Leishman, J. G., "Strobed Laser-Sheet Visualization of a Helicopter Rotor Wake," *Paper PF118, Proceedings of PSFVIP-2*, Honolulu, HI, May 1999.,

Also, *Journal of Flow Visualization & Image Processing* (in press).

¹¹Quackenbush, T. R., Bliss, D. B., and Wachspress, D. A., "New Free Wake Analysis of Rotorcraft Hover Performance Using Influence Coefficients," *Journal of Aircraft*, Vol. 26, No. 12, December 1990, pp. 1090–1097.

¹²Miller, W. O. and Bliss, D. B., "Direct Periodic Solutions of Rotor Free Wake Calculations," *Proceedings of the 46th Annual American Helicopter Society Forum*, Washington, DC, May 1990.

¹³Crouse, Jr., G. L. and Leishman, J. G., "A New Method for Improved Rotor Free Wake Convergence," *Presented at the 31st AIAA Aerospace Sciences Meeting and Exhibit*, Reno, NV, January 1993.

¹⁴Bagai, A. and Leishman, J. G., "Rotor Free-Wake Modeling Using a Relaxation Technique - Including Comparisons with Experimental Data," *Journal of the American Helicopter Society*, Vol. 40, No. 3, July 1995, pp. 29–41.

¹⁵Bagai, A. and Leishman, J. G., "Rotor Free-Wake Modeling using a Pseudoimplicit Relaxation Algorithm," *Journal of Aircraft*, Vol. 32, No. 6, Nov.-Dec. 1995, pp. 1276–1285.

¹⁶Bagai, A. and Leishman, J. G., "Free-Wake Analysis of Tandem, Tilt-Rotor and Coaxial Rotor Configurations," *Journal of the American Helicopter Society*, Vol. 41, No. 3, July 1996, pp. 196–207.

¹⁷Johnson, W., *Helicopter Theory*, Princeton University Press, 1980.

¹⁸Leishman, J. G., *Principles of Helicopter Aerodynamics*, Cambridge University Press New York, 2000.

¹⁹Truesdell, C., *The Kinematics of Vorticity*, chap. IV, Indiana Univ. Press Bloomington, IN, 1954, pp. 82–88.

²⁰Batchelor, G. K., *An Introduction to Fluid Dynamics*, Cambridge University Press Cambridge, UK, 1967.

²¹Bhagwat, M. J. and Leishman, J. G., "Stability, Consistency and Convergence of Time-Marching Free-Vortex Rotor Wake Algorithms," *Journal of the American Helicopter Society*, Vol. 46, No. 1, 2001 (to appear).

²²Conte, S. D. and de Boor, C., *Elementary Numerical Analysis : An Algorithmic Approach*, McGraw-Hill New York, 1980.

²³Laney, C. B., *Computational Gasdynamics*, Cambridge University Press New York, NY, 1998.

²⁴Bagai, A. and Leishman, J. G., "A Study of Rotor Wake Development and Wake/Body Interactions in Hover," *Journal of the American Helicopter Society*, Vol. 37, No. 4, October 1992, pp. 48–57.

²⁵Carpenter, P. J. and Fridovich, B., "Effect of A Rapid Blade-Pitch Increase on the Thrust and Induced-Velocity Response of a Full-Scale Helicopter Rotor," Tech. Rep. TN 3044, NACA, November 1953.

²⁶Munk, M. M., "Some Tables of the Factor of Apparent Additional Mass," Tech. Rep. TN 197, NACA, July 1924.

²⁷Ellenrieder, T. J. and Brinson, P. R., "The Dynamic Induced Velocity Field of a Model Rotor in Hover Conditions," *The Aeronautical Journal*, June/July 1998, pp. 331–335.